Dynamic control of embedded HVDC to contribute to transient stability enhancement

Juan Carlos Gonzalez-Torres, Valentin Costan, Gilney Damm, Abdelkrim Benchaib, Françoise Lamnabhi-Lagarrigue

Dynamic control of embedded HVDC to contribute to transient stability enhancement

Gonzalez-Torres Juan Carlos, Costan Valentin, Gilney Damm, Benchaib Abdelkrim, Lamnabhi-Lagarrigue Françoise

Dynamic control of embedded HVDC to contribute to transient stability enhancement

J.C. GONZALEZ-TORRES[1], V. COSTAN[2], G. DAMM[3], A. BENCHAIB[1], F. LAMNABHI-LAGARRIGUE[3]

[1] SuperGrid Institute SAS	[2]EDF	[3]L2S Lab
France	France	France

SUMMARY

The reinforcement of the transmission systems by means of HVDC systems, appears to be one of the most suitable solutions to face the challenges related to the evolution of power systems. In this context, this paper aims to investigate the impact of the overlaid HVDC systems on stability of the surrounding AC grid. More in particular, the rotor-angle transient stability problem is addressed.

Firstly, using a benchmark power system, it is shown that HVDC links controlled to track constant power references, do not intrinsically increase transient stability margins as an AC line naturally does. Such comparison highlights the need of supplementary control layers aiming the stability enhancement of the surrounding AC grid.

A proposed control strategy to improve the angle stability of the surrounding AC system is presented. The control is based on three identified actions HVDC systems allows: Injection of damping power, injection of synchronising power and fast compensation of power disturbances. These actions are then extrapolated to MTDC grids and implemented using a novel control structure. This structure allows to keep the zero power balance in every moment (DC voltage disturbances are minimal) while dealing with active power limits of the converters.

The proposed controllers are tested on the EMT-RV software using EMT models of all the devices in the grid. Simulation results allow to show the effectiveness of the proposed controllers for enhancing the rotor angle stability of the surrounding AC grid.

juan-carlos.gonzalez@supergrid-institute.com

KEYWORDS

Power system stability, HVDC Transmission, Hybrid AC/DC Transmission Grids, Transient stability, Multi-terminal DC grids, Wide Area Control System.

1 INTRODUCTION

The operation and structure of transmission systems is changing as the paradigms under which they were originally designed have evolved. This evolution has created new challenges for system operators such as the necessity to transmit bulk power over long distances. When this power transmission is done through long AC transmission lines, transient stability (the ability of the system to keep synchronism after being subject to a large disturbance) is one of the limiting factors [1]. One of the possibilities to overcome this challenge is the reinforcement of the transmission system. For this purpose, HVDC transmission has proven to be the most suitable technology since it overcomes some of the limitations of the AC lines. However, as shown in this paper, embedded HVDC systems used only for transmission purposes, don't intrinsically increase transient stability margins as an AC line naturally does. Control actions need to be performed in order to make the HVDC contribute to stability.

In this article, after showing the need of supplementary control layers for HVDC, a controller for active power modulations is presented. The control is based on three actions: damping power injection, synchronizing power injection and feed-forward actions. The control is applied on an HVDC in Point-to-Point configuration (PtP) embedded on a benchmark system. Then, the controller is implemented in a Multi-terminal HVDC grid (MTDC), taking into account the operational differences with respect to PtP configurations. All simulations in this paper are performed on EMPT-RV using the models of converters and cables described in [2]–[4].

2 STABILITY MARGINS OF HYBRID AC/DC TRANSMISSION GRIDS

In order to assess the transient stability margins, two modified versions of the Klein-Rogers-Kundur system [1] are compared. In the system in Figure 1(a) the two areas are interconnected through three identical AC lines. In the system in Figure 1(b), one of the AC lines is replaced by an HVDC link controlled in constant power mode. Converter connected to bus 7 controls the active power, while converter in bus 8 controls the DC voltage. The rated power of the converters is 350MVA. Compared with the original case, the exchanged power is increased to 450 MW, this power is equally distributed between the 3 lines in both cases (i.e. 150 MW per line).

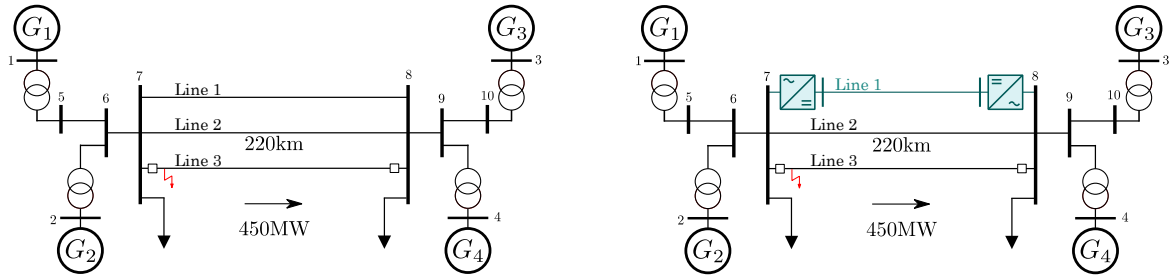

(a) AC system (b) AC/DC system

Figure 1. Modified Klein-Rogers-Kundur's two-area systems under comparison.

For the comparison, the simulated event is a three-phase fault on the third AC line near bus 7 at 1s, followed by the tripping of the line. Two different Clearing Times (CT, time span between fault occurrence and line tripping) are considered. Figure 2, shows the angle difference between the Center of Inertia [5] (COI) of Area 1 ($\delta_{COI,1}$) and the COI of Area 2 ($\delta_{COI,2}$) during the event. This value reflects the equivalent angular distance between both Areas. Figure 2(a) shows the systems response when the fault is cleared 110ms after fault occurrence (CT=110ms). Firstly, it is observed that the pre-fault angle difference is the same for both systems (20°), however during the first swing the AC/DC system presents higher angular deviations meaning that the AC/DC system is closer to system splitting. Furthermore, in the post-fault situation, the angle difference tends to a higher value in the AC/DC system, representing a more loaded situation on the remaining AC lines.

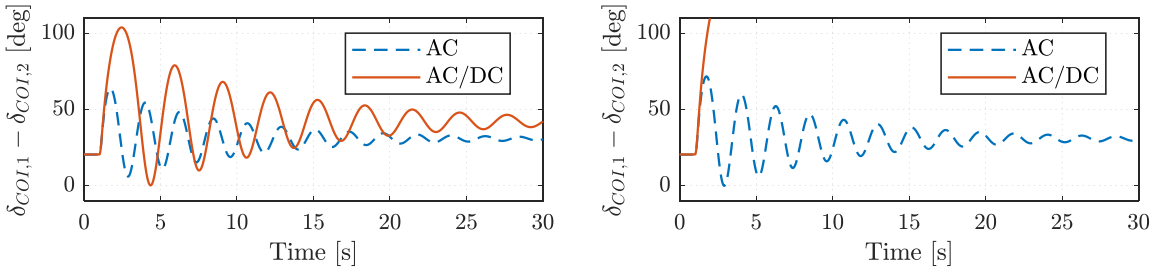

(a) Fault Clearing Time = 110ms (b) Fault Clearing Time = 130ms

Figure 2. Angle difference between areas.

Figure 2(b) shows the systems response when a CT of 130ms is considered. It is shown that such disturbance leads the AC/DC system to split, while the AC system remains in synchronism. Through iterative simulations, the Critical Clearing Times (CCT) are computed. The CCT for the AC system is 199ms while for the AC/DC system it is 120ms. These values indicate that in the **AC/DC case transient stability margins are smaller than in the AC case.** This phenomenon is due to the synchronizing nature of the AC lines, their synchronizing power injections (they transmit power as function of the transport angle) contribute to decrease the separation of areas. In the AC/DC case, as the HVDC link is set in constant power mode (150MW), its contribution against angle (or frequency) deviations is zero. It is evident that the fast control of the HVDC needs to be used for modulating the power references during electromechanical transients. As an AC line does, the available power headroom of the HVDC link can be used in order to increase the stability margins.

3 SUPPLEMENTARY CONTROL FOR HVDC SYSTEMS

To enhance transient stability a supplementary control layer for the HVDC link is proposed. This new layer of control means to modify the power references during electromechanical transients. Therefore, the power reference injected to the converter can be divided in two parts as follows:

$$P_{hvdc\_ref} = P_{hvdc0} + \Delta P_{hvdc}$$

where P_{hvdc0} is the power reference set by the TSO and ΔP_{hvdc} is the modulative part of the power reference used for stability enhancement. In order to get the most of the fast control of the HVDC link, three control actions are proposed to be combined, producing the following control law [6]:

$$\Delta P_{hvdc} = \overbrace{k_\delta(\theta_1 - \theta_2 - \bar{\theta})}^{ADC} + \overbrace{k_\omega(\dot{\theta}_1 - \dot{\theta}_2)}^{FDC} + k_{ff}\overbrace{(\text{Scheduled Power} - \text{Exchanged measured power})}^{Feedforward}$$

where θ_1 and θ_2 are angles reflecting the angle separation of the areas, $\bar{\theta}$ is an angle reference that can be dispatched by the operator as function of the scheduled power. $\dot{\theta}_1$ and $\dot{\theta}_2$ are instantaneous frequencies from the first and second areas and k_δ, k_ω and k_{ff} are the control gains.

The control can be described as the combination of the three following actions:

- **Angle Difference Controller (ADC):** This control action modifies the power reference proportionally to the angle difference (synchronizing power) in a similar way an AC line does. Synchronizing power injection enhances transient stability margins as an AC line (see comparison in Section 2). The angle reference $\bar{\theta}$ allows to make zero the ADC action in the pre-fault steady state. In addition to enhance transient stability, this action improve the static post-fault situation by modifying the steady-state power reference, thus unloading parallel AC lines [7]. In particular situations, this action allows to synchronise two power systems even in the absence of an AC interconnection.

- **Frequency Difference Controller (FDC):** This action modifies the power references proportionally to the frequency difference (injection of damping power). If the frequencies are measured at the Points of Common Coupling (PCC) of the converters, this strategy has proven to increase transient stability margins in every topological situation [8]. This action is also used to damp power oscillations if the measurements provide information about the oscillation [9].

- **Feedforward Action:** Through the fast response of the converters, it is possible to compensate power disturbances in the grid if they are known [10]. For example, if a parallel line is tripped, the power can be rapidly reallocated in the HVDC link. If fast power injections in one area occur (e.g. fast frequency response), this action can be used to rapidly share those injections between areas.

In addition of enhancing transient stability, the combination of these actions allows to modify the dynamic behaviour of the interarea oscillation by the correct tuning of the control gains.

3.1 Supplementary control for an embedded point-to-point HVDC

For the two-area AC/DC system in Figure 1(b) the active power references of the HVDC link are modulated around the steady-state set-point using the proposed controller, implemented as follows:

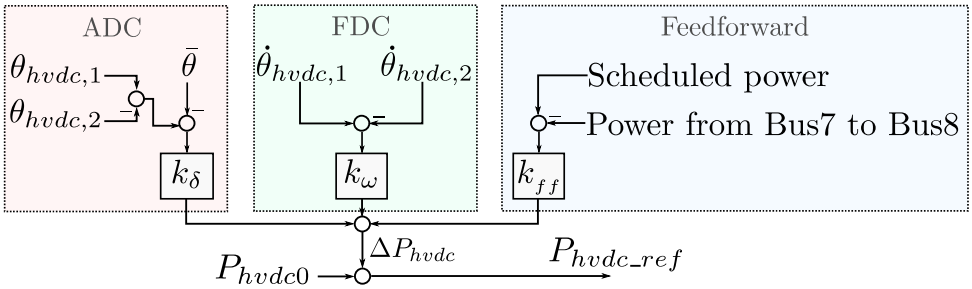

Figure 3. Control implementation for an HVDC link

The values $\theta_{hvdc,1}$ ($\dot{\theta}_{hvdc,1}$) and $\theta_{hvdc,2}$ ($\dot{\theta}_{hvdc,2}$) correspond to the phase angles (frequency) at the PCC of each converter (i.e. bus 7 and bus 8). Measurements of angles and frequencies are done using PLL-based models of Phasor Measurement Units (PMUs). The scheduled exchanged power between areas is 450MW and the reference angle is $\bar{\theta}$=20deg.

To test the controller, the fault clearing time considered in this example is CT=200ms. The three sets of gains summarized in Table 1 are considered. Case 0 represents the case without supplementary control (as in Section 2). In Case 1 the value of the synchronizing gain (k_δ) is higher than in Case 2, while the damping gain (k_ω) in Case 2 is higher than in Case 1. Figure 4 shows the system response for both configurations.

Regarding the stability margins, while system in Case 0 splits after a 200ms fault (since CCT=120ms, see Section 2), the systems with supplementary control remain stable as shown in Figure 4. The CCTs for Cases 1 and 2 are summarized in Table 1, it can be seen that these CCTs are even than the CCT of the case with three AC parallel lines (CCT=199ms, system in Figure 1(a)). It also must be noted that the choice of the gains can drastically modify the damping and frequency oscillation of the interarea oscillations present after fault clearing. For example, oscillations in Case 2 are better damped than Case 1 due to the higher value of the damping gain, while frequency of oscillations in Case 1 are faster than in Case 2 due to the higher value of the synchronizing gain [11].

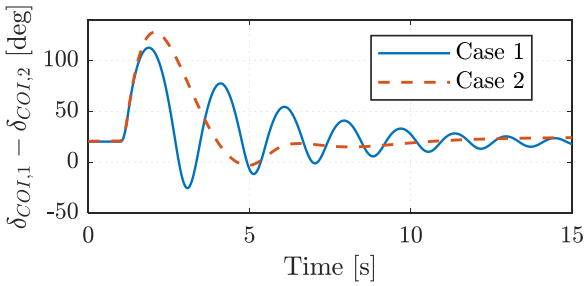

Figure 4. Angle difference between areas

Case	Control Gains			CCT [ms]
	k_δ [MW/deg]	k_ω [MW/Hz]	k_{ff} [MW/MW]	
0	0	0	0	120
1	17.9	102	1	235
2	1.61	430	1	230

Table 1. Control gains and CCTs

Figure 5 shows the active power flowing through the HVDC as well as that passing through the AC lines. In the pre-fault situation the 3 lines transport the same amount of active power, during the fault transmitted power is zero until line 3 is tripped. After fault clearance, the power flowing through the HVDC link is modulated thanks to the controller. In Case 1, the control effort during the first swing is higher (even reaching converter limits) than in Case 2, this explains the smaller angle deviation in Figure 4. It is noted that in Case 1, HVDC power modulations are in phase with the power oscillations of the AC line (higher synchronizing gain), while in Case 2 modulations are in opposite phase, providing damping power injections (higher damping gain).

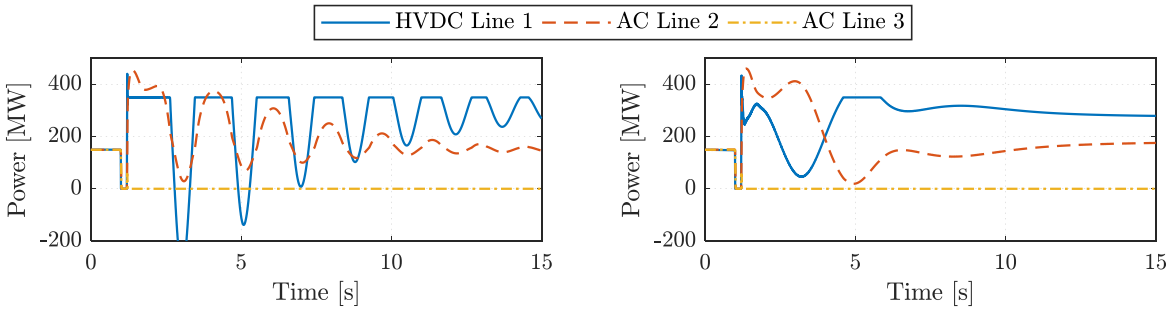

(a) Case 1: Predominant synchronizing gain

(b) Case 2: Predominant damping gain

Figure 5. Active power through the AC/DC corridor. The rated power of the HVDC is 350MVA

Moreover, the feedforward action reallocates the power of the tripped line on the HVDC link, leading the HVDC link to double its power transmitted in the post-fault steady state. Additionally, after the disturbance, angle deviation tends to its pre-fault situation, leading the AC line to transport the same power as in the pre-fault steady state. The fast power reallocation can imply a severe power reference variation, therefore controllers allowing fast power reference modulations while keeping the stability of the DC systems are recommended (e.g. [4], [12]).

4 SUPPLEMENTARY CONTROL FOR MTDC GRIDS

4.1 Operational differences between MTDC grids and HVDC links

Inside the DC grid of an HVDC systems (point-to-point or in MTDC), the DC voltages are an indicator of the balance between power injections and extractions, thus a requirement for the correct operation of the system is to keep the DC voltage within an acceptable range. In VSC-HVDC links, control of DC voltage is managed by one station (master), evacuating all the power injected by the other station (slave). In MTDC grids it is preferred to use the DC voltage droop control which allows multiple stations to participate in the voltage control.

In a situation where multiple HVDC links are used to enhance rotor angle stability, the number of independent active power references is equal to the number of HVDC links. If an MTDC is used to

enhance stability of the AC system, the number of independent active power references is equal to the number of connected stations minus one. In other words, for the same amount of converters, an MTDC provide some extra degrees of freedom, however the supplementary power modulations should be generated in a coordinated manner to guarantee the zero power balance.

Other difference concerns the power limits of the converters. In a PtP, both converters have the same rated power, if power references saturate the slave converter, the master is still able to evacuate the power. In an MTDC, the stations can have different rated powers, so if at least one converter is saturated, the stability of the DC voltage can be at risk. Thus, the supplementary controls need to guarantee the zero power balance even if converters reach their limits.

4.2 The supplementary control

In order to handle the aforementioned challenges in MTDC grids, a new control structure is proposed. The idea behind the structure is that if converter i modulates its power in one direction, Converter j modulates the same amount of power in the opposite direction. Through the coordination of references by pair of converters, this structure allows to apply a desired control law, while keeping the zero power balance even if converters reach their limits.

As an example, consider the 3-terminal embedded MTDC grid in *Figure* 6. The three power set-points of the operator are set to zero. Consider the power of Converters 1 and 2 are modulated proportionally to the angle difference between bus 1 and 2, as follows:

$$\Delta P_{hvdc,1} = k_{\delta,12}(\theta_{hvdc,1} - \theta_{hvdc,2}) \quad \text{and} \quad \Delta P_{hvdc,2} = k_{\delta,21}(\theta_{hvdc,2} - \theta_{hvdc,1})$$

It is clear that if $k_{\delta,12} = k_{\delta,21}$, the same amount of power injected by Converter 1 will be extracted by Converter 2, preserving the zero power balance in the DC grid. Moreover, from the AC grid perspective, an amount of power is extracted from bus 1 and injected in bus 2 (similar to an AC line), passing it through the DC grid. In general, from the AC grid perspective, each pair of converters ij can be interpreted as an unified actuator, called here ***Virtual link ij***, transporting power from the AC bus i to the AC bus j (as a PtP does), independently of the DC grid topology.

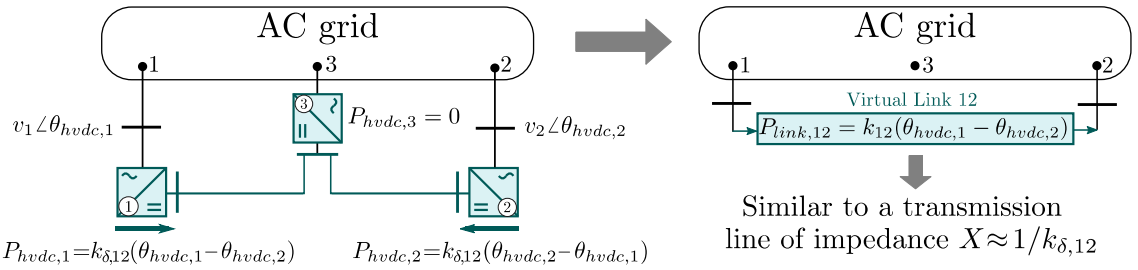

Figure 6. Example of a *virtual link* between Stations 1 and 2

The concept of *virtual link* can be used to apply any control law between each pair of converters. To be consistent, in this article the ADC and the FDC are applied to control power injections of an MTDC. Therefore, in order to be general, consider an MTDC composed of n converters embedded into an AC grid, the power reference for the $i-th$ converter is given by:

$$P_{hvdc\_ref,i} = P_{hvdc0,i} + \Delta P_{hvdc,i}$$

where $P_{hvdc0,i}$ is the desired set-point and $\Delta P_{hvdc,i}$ is the supplementary reference given by the controller. In order to apply the FDC and the ADC between each pair of converters, the supplementary reference of the Converter i is given by:

$$\Delta P_{hvdc,i} = \overbrace{\sum_{j=1}^{n} k_{\omega,ij}\left(\dot{\theta}_{hvdc,i} - \dot{\theta}_{hvdc,j}\right)}^{FDC} + \overbrace{\sum_{j=1}^{n} k_{\delta,ij}(\theta_{hvdc,i} - \theta_{hvdc,j} - \bar{\theta}_{ij})}^{ADC}$$

$$\text{with} \quad k_{\omega,ij} = k_{\omega,ji} \quad ; \quad k_{\delta,ij} = k_{\delta,ji}$$

where $\theta_{hvdc,i}$ ($\dot{\theta}_{hvdc,i}$) is the phase angle (instantaneous frequency) measured at the PCC of the Converter i. The value $\bar{\theta}_{ij}$ is a reference for the angle between the PCCs of Converters i and j. $k_{\omega,ij}$ and $k_{\delta,ij}$ are the control gains for each *virtual link* ij. As in the PtP configuration, in order to enhance transient stability, the FDC injects damping power between each pair of converters, while the ADC injects synchronizing power. It has been stated that in PtP, the ADC can be considered as the emulation of an AC line (as depicted in Figure 6), thus in MTDC, when the ADC is applied between more than 2 converters, it can be interpreted as the emulation of a set of AC lines.

In order to preserve the zero power balance in the grid when converters reach their limits, in this structure it is proposed to limit the reference of each *virtual link ij*, locally at each converters level. The set of constraints that must be fulfilled is defined by the fact that the sum of powers of the *virtual links* "connected" to a converter shouldn't exceed the power limits of the converter. For a better understanding, an example of implementation is done in the following section.

4.2 Example

The proposed control has been implemented and tested on a modified version of the New England IEEE 39-Bus System. A radial MTDC grid is installed in the test system connecting buses 2, 22 and 29, as shown in Figure 7. With respect to the original case, a 450 MW load is connected to bus 2, Generation of G9 is increased by 200 MW and G6 is increased by 250 MW.

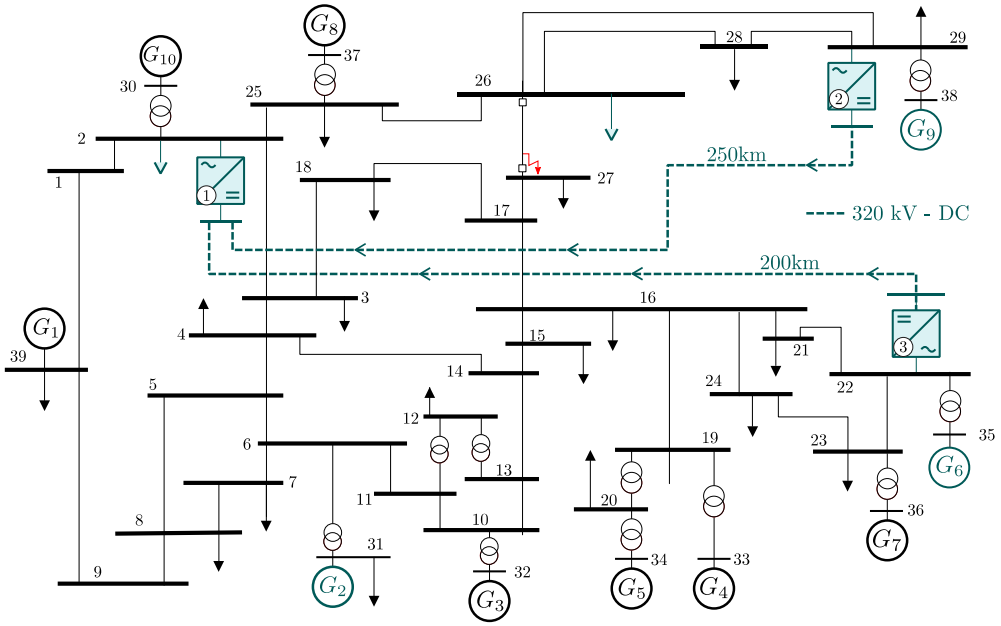

Figure 7. Modified version of the IEEE 39-bus system

The rated power of the converters, as well as their initial conditions are summarized in Table 2. The voltage angles suggest that the tendency of the power-flow is from the right part to the left part of the system (from Converters 2 and 3 to 1). The positive and negative headroom of the converter ($\Delta P^{max}_{hvdc,i}, \Delta P^{min}_{hvdc,i}$) are the difference between the rated power and the active power set-point.

Converter i	PCC Voltage [pu]	Rated power [MVA]	$P_{hvdc0,i}$ [MW]	$Q_{hvdc0,i}$ [MVAR]	$\Delta P^{max}_{hvdc,i}$ [MW]	$\Delta P^{min}_{hvdc,i}$ [MW]
1	$1\angle 0°$	700	-450	100	1150	-250
2	$1.05\angle 15.24°$	400	200	60	200	-600
3	$1.01 \angle 6.8°$	400	250	60	150	-750

Table 2. Converters characteristics and set-points

The implementation of the controller on Converter 1 is depicted in Figure 8 (all converters are equipped with an equivalent one). The control receives frequency and angle measurements from other stations to apply the ADC and FDC. The ADC and FDC action of each pair of converters (or *Virtual link*) are limited to a value ($P^{max}_{link,ij}$, $P^{min}_{link,ij}$) and recombined to generate the power reference of the station. The limits of each *virtual link* are summarized in Table 3. They are designed to respect the available headroom of the converters (e.g. $\Delta P^{max}_{hvdc,1} \geq P^{max}_{link,12} - P^{min}_{link,31}$). It must also be noted that the limits of a *virtual link ij*, are applied to the *virtual link* reference in Converter i as well as in Converter j.

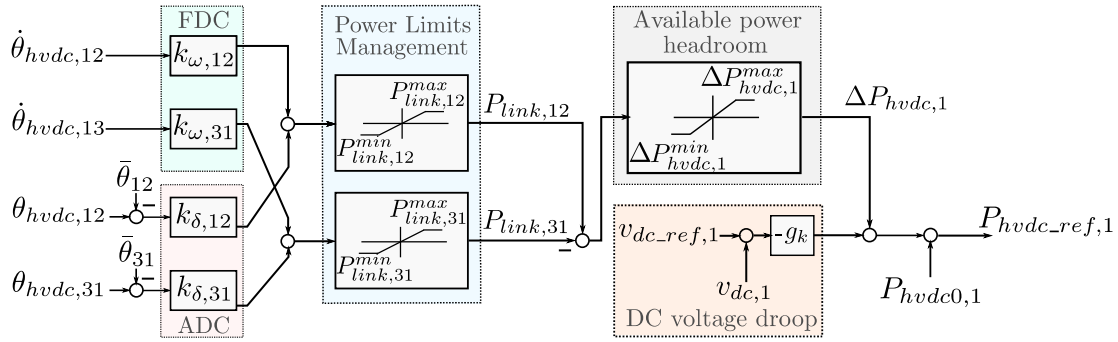

Figure 8. Control implementation on Converter 1

Virtual Link ij	$k_{\omega,ij}$ [MW/Hz]	$k_{\delta,ij}$ [MW/deg]	$\bar{\theta}_{ij}$ [deg]	$P^{max}_{link,ij}$ [MW]	$P^{min}_{link,ij}$ [MW]
12	500	10	-15.24	600	-100
23	500	10	8.44	100	0
31	500	10	6.8	150	-550

Table 3. Control gains

In order to test the controller, a three-phase fault is simulated in line 26-27 near bus 27 followed by the tripping of the line. For the analysis, different Clearing times are considered in the following.

Severe fault (CT=140ms): In a first example, the line is tripped 140ms after fault occurrence. Figure 9(a) shows the angle separation between G9 and G1 for two situations: In the first one no supplementary control is used (CR for constant references), in the second one, the proposed control is implemented (ADC-FDC). When no supplementary control is implemented (CR), it is shown that the fault leads to the separation of generator G9. In the other hand, the implementation of the ADC-FDC strategy manages to keep the system in synchronism.

Figure 9(b) shows how active power is modulated to keep the system stable. During the first swing, Converters 1 and 2 reach their limits during some milliseconds (approximately between t=700ms and t=950ms). During this time span, Converter 3 stops the power modulations, even if it has still some available headroom (approx. 100MW). Thanks to this action, the discharge of the DC grid is avoided. In Figure 9(c) it can be seen that the DC voltages remain by far into an acceptable range

of ±10% of the nominal voltage. Note that Converter 3 stops to modulate power thanks to the limitation of the *virtual links in* Figure 9(c). It is shown that during the mentioned time span, all the *virtual link* references are saturated, therefore all power references stop their modulations.

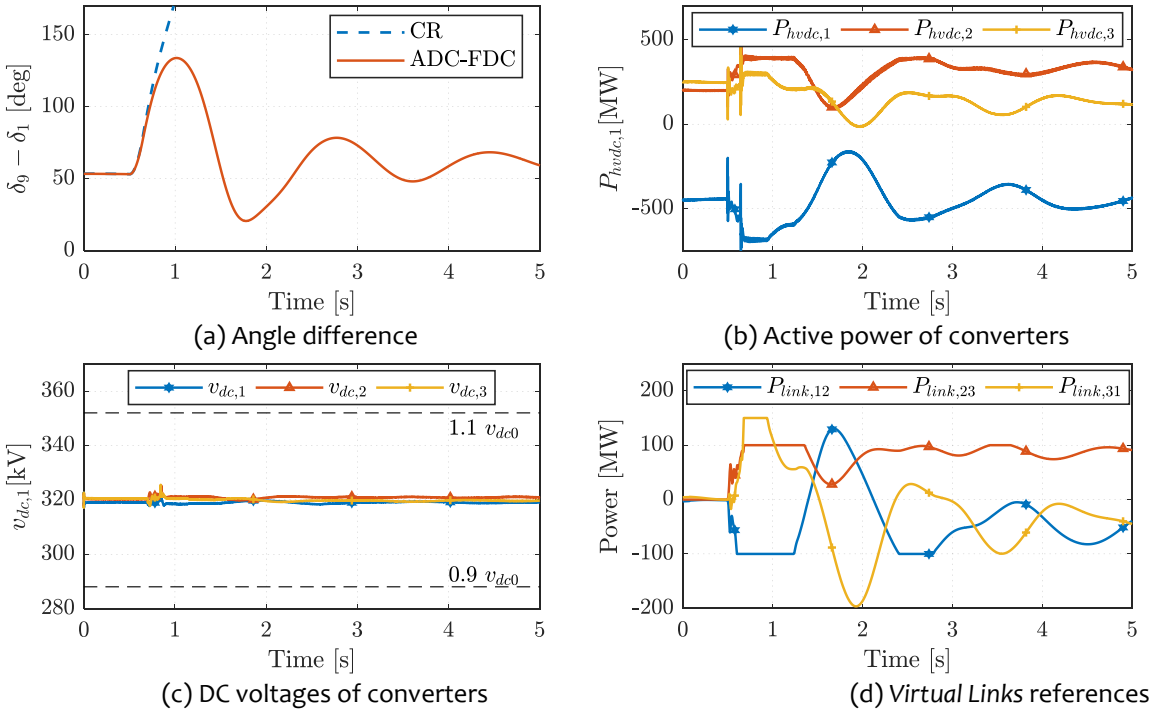

(a) Angle difference (b) Active power of converters

(c) DC voltages of converters (d) *Virtual Links* references

Figure 9. System response after a 140ms three phase fault

It is also clear that, the value of the power references in the post-fault steady state are not the same as before the fault, especially for Converters 2 and 3. This is due to the ADC, which emulates AC lines between converters. Angle separations are bigger after the fault, so the ADC makes Converter 2 to "send" more power to Converter 3 to keep both buses closer. It can be seen that the *virtual link* 23 "sends" around 100MW in the post-fault steady state.

Less severe fault (CT=100ms): In this example, the fault location is the same, but the line is tripped 100ms after fault occurrence. Figure 10 show the angle difference between PCCs, for both strategies. It is shown that in the CR strategy, during the first swing, angles deviate more than in the FDC-ADC case. More important is to appreciate that in the static post-fault situation, when FDC-ADC is implemented, angles tend to remain closer from each other. This means that surrounding AC lines are in a less stressed situation than in the CR case. This example shows the usefulness of the FDC-ADC control, not only for transient stability enhancement, but also for static purposes.

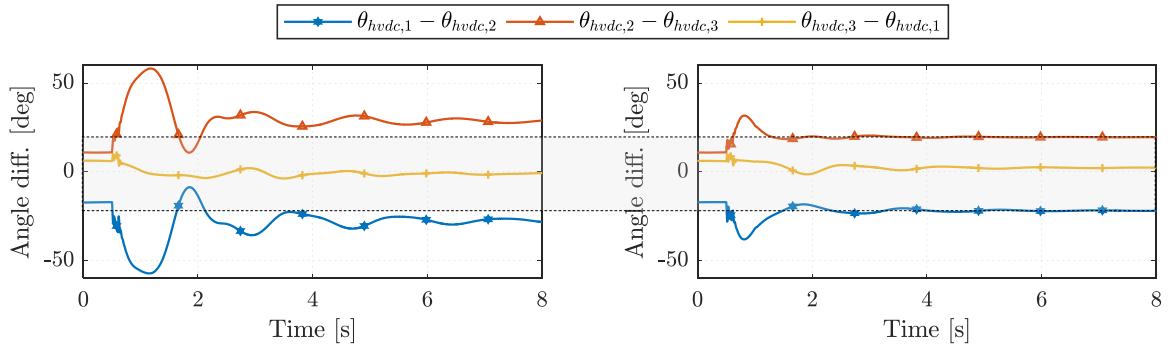

(a) Constant References (CR) (b) FDC+ADC strategy is implemented

Figure 10. Angle separations using different strategies after a 100ms fault

CONCLUSIONS

This paper proposes supplementary controllers for active power modulations of embedded HVDC systems allowing to enhance the transient stability of the surrounding AC system. It has been proved that HVDC systems controlled in constant power mode, do not intrinsically increase transient stability margins as an AC line naturally does. Therefore supplementary controllers as the one presented in this paper are necessary.

The proposed controllers are based on the injection of damping and synchronising power as well as the compensation of power disturbances. These controllers use measurements of angles, instantaneous frequencies and powers flowing in the AC network. For the MTDC configuration a new decentralized control structure is presented. This structure uses the concept of *Virtual Links* in order to assure the zero power balance of the MTDC grid even when converters reach their limits. EMT simulation results, using benchmark power systems, show the effectiveness of the proposed controllers in PtP as well as in MTDC configuration. It has been also shown how this controllers are effective not only for transient stability enhancement, but also for static purposes.

BIBLIOGRAPHY

[1] P. Kundur, *Power System Stability And Control*. New York: McGraw- Hill, 1994.

[2] K. Shinoda, A. Benchaib, J. Dai, and X. Guillaud, "Virtual Capacitor Control: Mitigation of DC Voltage Fluctuations in MMC-Based HVdc Systems," *IEEE Trans. Power Deliv.*, vol. 33, no. 1, pp. 455–465, 2018.

[3] D. Loume, M. N. Tuan, A. Bertinato, and B. Raison, "DC cable modelling and High Voltage Direct Current grid grounding system," *9th Int. Conf. Insul. Power Cables*, no. April, pp. 1–6, 2015.

[4] A. Zama, A. Benchaib, S. Bacha, D. Frey, and S. Silvant, "High Dynamics Control for MMC Based on Exact Discrete-Time Model With Experimental Validation," *IEEE Trans. Power Deliv.*, vol. 33, no. 1, pp. 477–488, 2018.

[5] H.-D. Chiang, *Direct Methods for Stability Analysis of Electric Power Systems*, vol. 12, no. 5. Hoboken, NJ, USA: John Wiley & Sons, Inc., 2010.

[6] J. C. Gonzalez-Torres, V. Costan, G. Damm, A. Benchaib, and F. Lamnabhi-Lagarrigue, "Procède de commande d'un lien de transmission électrique incluant une ligne haute tension continu," 2018.

[7] L. Coronado *et al.*, "INELFE: main description and operational experience over three years in service," in *2019 AEIT HVDC International Conference (AEIT HVDC)*, 2019, pp. 1–6.

[8] L. Sigrist, F. Echavarren, L. Rouco, and P. Panciatici, "A fundamental study on the impact of HVDC lines on transient stability of power systems," in *2015 IEEE Eindhoven PowerTech*, 2015, pp. 1–6.

[9] J. C. Gonzalez-Torres, J. Mermet-Guyennet, S. Silvant, and A. Benchaib, "Power system stability enhancement via VSC-HVDC control using remote signals: Application on the Nordic 44-bus test system," *IET Conf. Publ.*, vol. 2019, no. CP751, pp. 1–6, 2019.

[10] R. Eriksson, V. Knazkins, and L. Soder, "On the assessment of the impact of a conventional HVDC on a test power system," in *2007 iREP Symposium - Bulk Power System Dynamics and Control - VII. Revitalizing Operational Reliability*, 2007, pp. 1–5.

[11] J. Renedo, L. Rouco, L. Sigrist, and A. Garcia-Cerrada, "Impact of AC-line-emulation controllers of VSC-HVDC links on inter-area-oscillation damping," in *IECON 2019 - 45th Annual Conference of the IEEE Industrial Electronics Society*, 2019, pp. 4825–4830.

[12] K. Shinoda, A. Benchaib, J. Dai, A. Zama, B. Luscan, and X. Guillaud, "Virtual capacitor for DC grid stability enhancement," in *CIGRE 2018*, 2018, pp. 1–6.